Identifying and Simulating Hydrogen in the Galactic Center Outflow

Savannah Cary, Wellesley College
Advisor: Jay Lockman, Green Bank Observatory

August 2020

Abstract

During this project we identified approximately 50 new clouds in regions previously observed by the GBT. An additional set of data was released earlier this year, containing clouds with particularly high velocities that did not fit previous kinematic models highlighted in the Lockman et al. 2020 paper. To solve this issue, we found that the outflow must be accelerating for longer and is much older than previously predicted. Furthermore, a noticeable gap in VLSRs of clouds at high latitudes could be attributed to an episodic outflow, although the same outcome could be due to clouds evaporating in the winds and becoming too faint to observe. Other work this summer includes analyzing cloud morphology, as well as finding clouds exhibiting "comet"-like features that may be fundamental to understanding how the nuclear winds develop.

1 Introduction

The existence of galactic nuclear wind, both in neighboring galaxies and our own Milky Way, has been discussed since the early 2000s (e.g., Bland-Hawthorn and Cohen 2003; Veilleux et al. 2005; Keeney et al. 2006). Two lobes extending from the Milky Way have been detected in the γ-ray, extending to latitudes $|b| = 55^\circ$ and ≈ 8 kpc below and above the galactic center; they are referred to as the Fermi Bubbles (Su et al. 2010). Having been generated by energetic processes through either star formations or an active galactic nucleus (AGN), the Fermi Bubbles give us the opportunity to study phenomena in the galactic nuclear wind up close and in more detail than for other galaxies.

Spectral observations have detected 21cm Hydrogen emission in the Fermi Bubbles (McClure-Griffiths et al. 2013; Di Teodoro et al. 2018). Current models show that these neutral hydrogen clouds are accelerating in the Fermi bubble wind, starting at 150 km/s close to the Galactic Center and rise to 330 km/s in a few kiloparsecs away from the center (Lockman et al. 2020). In this paper, we consider the clouds that do not fit the model presented by Lockman et al. 2020, specifically clouds at $V_{LSR} \gtrsim 300$ km/s.

This report will begin with Section 2 outlining theory and equations for the kinematics of the clouds. Section 3 will introduce the new clouds, and highlight questions we have of trends found in the complete set of data. Section 4 will focus on simulations in an attempt to explain these observations. Section 5 presents other work during this summer that don't fit into the previous categories. Section 6 is the conclusion.

In this paper, the adopted Sun-center distance will be R_0= 8.2 kpc and LSR rotational velocity to be $|V_0|$=240 km/s.

2 Theory and Procedures

2.1 Positions and Velocities of Clouds

Properly analyzing the outflow requires understanding how observed quantities relate to coordinates with respect to the galactic center. Figure 1 shows the defined coordinate system.

Data simulated in this report were generated in rectangular coordinates with respect to the galac-

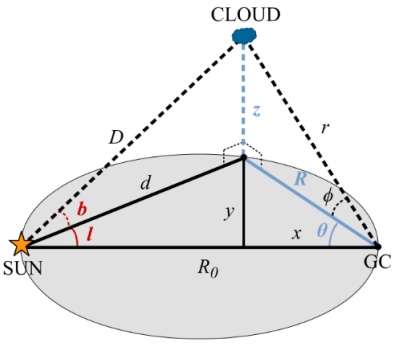

Figure 1: The definition of the coordinate system used, found in Di Teodoro et al. 2018. Solid lines lie in the galactic plane at z = 0. Cylindrical coordinates are represented as (R, θ, z), spherical as (r, θ, ϕ), and cartesian as (x, y, z). Theta is a right handed system that is aligned with $\ell = 0$. The distance to the galactic center is $R_0 = 8.2$ kpc, with D representing the cloud's distance from the sun and d representing the projection on the Galactic Plane. Galactic longitude and latitude are designated as b and ℓ, respectively.

tic center. In order to transfer the clouds' space velocities and positions into observable quantities, the following equations are needed. Latitude ℓ and longitude b are described as:

$$\ell = arctan(\frac{y}{R_0 + x}) \quad (1)$$

$$b = arctan(\frac{z}{d}) \quad (2)$$

A cloud in the Fermi Bubbles will have an outflow velocity $V_{(\theta,R,z)}$. With the Sun's LSR rotational velocity $V_\odot$, the observed V_{LSR} is as defined as the following:

$$V_{LSR} = (V_\theta \frac{R_\odot}{R} - V_\odot) sin(\ell) cos(b) + V_z sin(b) - V_R cos(\ell + \theta) cos(b) \quad (3)$$

Figure 2 shows the effect of how the clouds space velocities are projected as LSR velocities if the wind was a constant velocity. The closer the cloud is to the solar system, the more blue shifted it is. Alternatively, if the cloud lies on the far side of the Fermi Bubbles, it will be observed to be red shifted. The conical region in Figure 2 is a representation of the observational volume. As the cone extends to the far side of the lobes, more clouds with positive velocities are able to be observed. In the case of an outflow, we expect to observe more positive velocity clouds than negative.

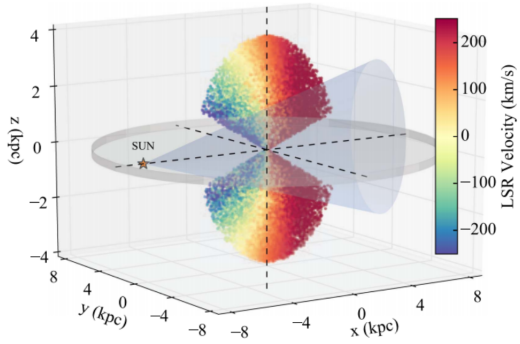

Figure 2: An outflow with a constant velocity of 330 km/s, as shown in Di Teodoro et al. 2018. The clouds are color coded by LSR velocity. The cone with the apex centered on the sun represents the volume observed through the GBT.

2.2 The 21 cm HI Data

The 21 cm HI data were taken with the Green Bank Telescope and Australian Telescope Compact Array. The clouds from these data sets can be found in McClure-Griffiths et al. 2013, Di Teodoro et al. 2018, and Lockman et al. 2020. This summer's work derived a more completed list of clouds, both by adding new clouds and removing those that turned out to be duplicates or non-existent.

The final product of the 21 cm data observed is in the form of a data cube, with each pixel a measure of brightness temperature. The cube has dimensions of galactic latitude, galactic longitude, and V_{LSR}

2.3 Calculating Masses

This summer, we also needed to calculate the masses of the new set of clouds. CASA was used to view the datacube, yet there were errors in the program when attempting to fit a gaussian to the spectral profile of the clouds. Two spectral profiles were exported per cloud: one averaged over

the region containing the cloud, and one at the location of the max brightness temperature, $T_{b,peak}$. With peak average temperature of the region profile being $T_{r,peak}$ and full width at half maximum (FWHM) Δv, the total column density of HI atoms N_{HI} is:

$$\langle N_{HI} \rangle = 1.82e18 \; T_{r,peak} \; \Delta v \; 1.065 \; (cm^{-2}). \quad (4)$$

The number of pixels contained in the defined region is N_{pix}, the area per pixel is A, and the angular size of a pixel is $\gamma = 105$". All clouds are assumed to have the same distance $D = R_0 = 8.2$ kpc. With the mass of a hydrogen atom as m, the mass M_{HI} is described by the following:

$$A = (Dsin(\gamma))^2 \quad (5)$$

$$M_{HI} = mN_{pix}\langle N_{HI} \rangle A \quad (6)$$

3 Finding New Clouds

A large component of this project was identifying false clouds in the data, as well as collecting data for clouds that were missed by the pre-existing cloud-finding algorithm. Overall, 47 new clouds were found this summer. It is possible that some of these clouds were not detected before due to their blending with other line components. An example is in Figure 3(a). However, this only accounted for 7 clouds. Other clouds had a more well-defined spectrum, an example being Figure 3(b).

With the clouds detected both during this summer and earlier this year, we were able to identify certain trends in the data not previously exposed.

3.1 Lack of Asymmetry in Velocities

As mentioned in Section 2, because of projection effects, we expect to have more positive velocity clouds than negative velocity clouds in an outflow. However, this is not what we observed in our data. In fact, there are 131 negative velocity clouds and 116 positive velocity clouds, a lack of asymmetry that can be explained. The Fermi Bubbles are quite large, and recalling Figure 2, the positive V_{LSR}s would be found on the far side of the Fermi Bubbles, some nearly double the distance as clouds on the near side of the lobes. The negative velocity clouds are much easier to detect due to their proximity to us, but the positive velocity clouds would be much fainter due to being further from us. For now, this is not a topic of concern.

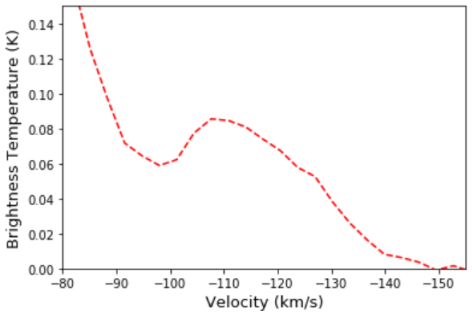

(a) Merged Spectrum

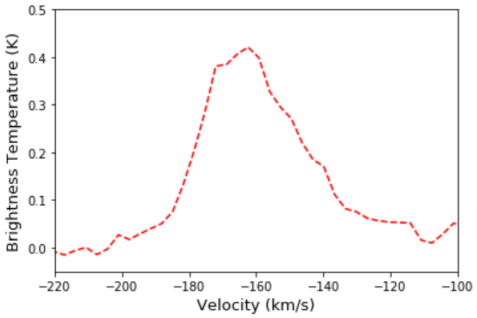

(b) Defined Spectrum

Figure 3: Two examples of spectra found in the data set from this summer. Figure (a) represents a spectral profile that's blended with VLSR =0 emission. Figure (b) shows a profile that is not blended.

3.2 Lack of Mid-Velocities at High Latitudes

With the new clouds, an obvious gap in velocities at high latitudes has emerged; as seen in Figure 4. We sought to explain what this gap meant and why it would have appeared.

3.3 Additional High Velocity Cloud

In the previous acceleration models, the HI clouds in the outflow accelerated to VLSRs of approximately 300 km/s (Lockman et al. 2020), as represented by Figure 5.

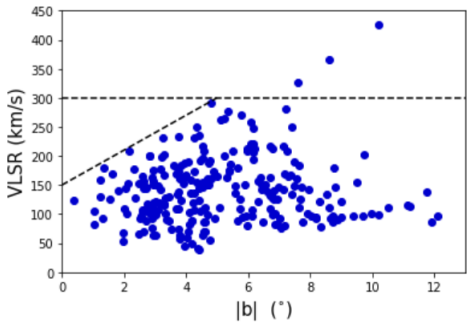

Figure 4: All of the clouds up to date. The dashed line at 300 km/s represents the threshold of velocities from the Lockman et al. 2020 paper, whereas the vacant triangular region represents an accelerating wind.

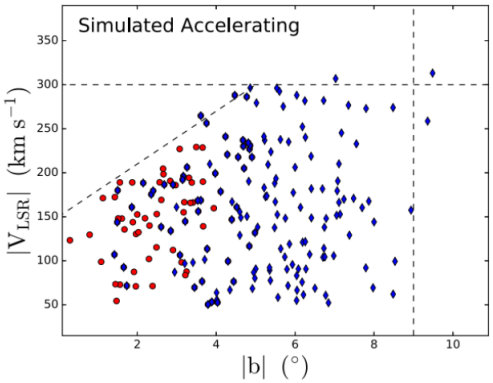

Figure 5: Graph from Lockman et al. 2020 simulating an accelerating outflow. The dashed lines show where the clouds are limited to in the simulation. The triangular region with absent clouds is due to acceleration of the winds, whereas the dashed line at 300 km/s shows the velocity limits of this simulation. Red dots show what would have been observed by ATCA, and blue diamonds show what would have been observed by the GBT.

However, this excluded a cloud found at a velocity of 365.9 km/s. Earlier in the year, a set of 20 new clouds were detected that included another high velocity cloud at 425 km/s. Part of this summer's work was generating a new model for acceleration that could explain these high velocity clouds.

4 Simulations of the Galactic Winds

In order to help explain the questions above, we created various simulations that modeled the outflow. These simulations were produced using Vpython. Clouds were generated from the galactic center,(0,0,0), every .01 MYR for all simulations. They were then given a constant acceleration, leaving the velocities to be dependent on time since ejection. The clouds were uniformly ejected within a cone to represent the Fermi Bubbles.

Other modeling work this summer included simulating a starburst region, where the clouds were released with x,y offsets. Additionally, we began work on including a change in acceleration either through including jerk or gravity as the clouds outflow away from the galactic plane. However, other work is anticipated on these simulations to produce conclusive results.

4.1 Acceleration

The first step in simulating was to accelerate the clouds on the same timescale as previously recorded, but change the acceleration in order to reach VLSRs of 425 km/s. Past data set the maximum age of the clouds to be approximately 8 MYR (Di Teodoro et al. 2018). Therefore, that is the age that the first model adopted. To achieve high velocities, the necessary minimal acceleration was found to be .0600 kpc/MYR/MYR, or 58.7 km/s/s. Figure 6 shows the latitude vs V_{LSR} graph produced

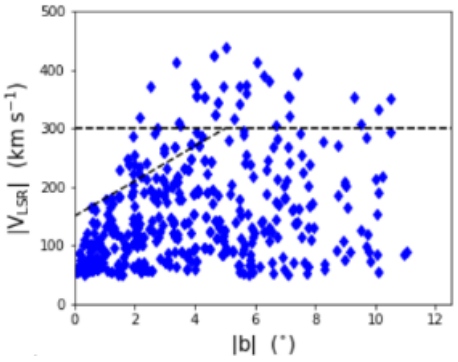

Figure 6: Latitude vs Velocity graph of the simulated clouds with max age 8 MYR and acceleration .060 kpc/MYR/MYR

from this set of simulated clouds. Here, it is obvious the simulated clouds do not follow the same trend as the observed clouds in Figure 4. The high velocities are reached at much lower latitudes in the simulation than in the data. In addition, the greatest longitude value produced is 12° whereas the data extends to longitudes 16°. The next step in simu-

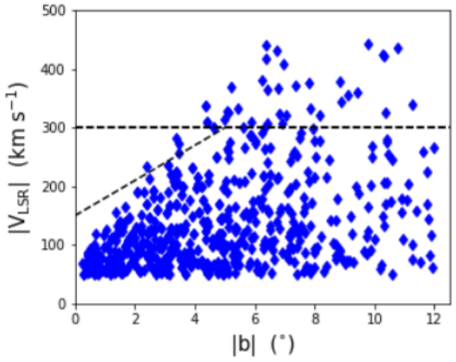

Figure 7: Latitude vs Velocity graph of the simulated clouds with max age 20 MYR and acceleration .0275 kpc/MYR/MYR

lating was to change both the acceleration and the age of the clouds. The model that worked best was setting an acceleration of .0275 kpc/MYR/MYR, or 26.9 km/s/s, and having the clouds accelerate for 20 MYR rather than 8. Figure 7 shows the resulting V_{LSR} vs latitude graph. The overall trend is similar to the observed data, where the high velocity clouds are observed at higher latitudes. However, there are higher velocity clouds present at slightly lower latitudes, such as 6°. Although this simulation does not perfectly fit the observed data, it does suggest that the hydrogen clouds have been accelerating in the outflow for much longer than previously expected.

This simulations suggest a cloud lifetime of 20 MYR, yet other studies show that if the current bubbles of x-rays and γ-rays were produced by an AGN, they would be 2-8 MYR old (Bland-Hawthorn et al. 2019). Studies suggesting that the galactic nucleus undergoes periodic bursts (e.g., Guo & Mathews 2012; Bland-Hawthorn et al. 2019). This could be a possible explanation for this discrepancy between ages. An episodic outflow is also supported by the simulation in the following section.

4.2 An Episodic vs Continuous Outflow

A question that arose during the summer was whether this outflow was continuous or episodic. The previous acceleration models in section 4.1 were continuous. Using the 20 MYR model from section 4.1, we removed clouds that were between the ages of 12 and 16 MYR to represent a period of time where no clouds were being produced. The leftover clouds had ages of less than 12 MYR and greater than 16 MYR. A plot of velocity vs latitude

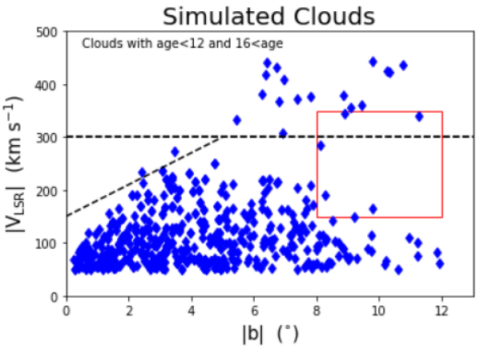

(a) Simulated Clouds

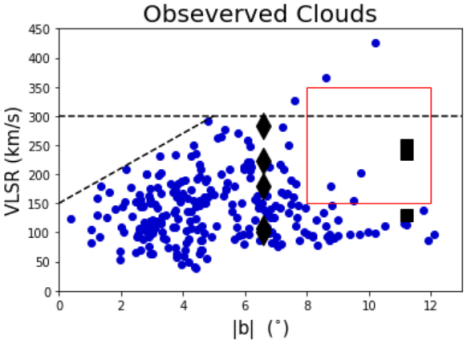

(b) Observed Clouds

Figure 8: The blue dots represent the HI clouds up to date. In Figure (b), the black diamonds and squares are UV data from Savage et al. 2017 and Fox et al. 2015, respectively. The red boxes are in the same position on both graphs, representing a region absent of clouds.

of these simulated clouds is given in Figure 8 (a), and a plot of the observed clouds is given in Figure 8 (b). The simulated data shows an absence of clouds in the same area as seen by the actual data. However, there is also an absence of clouds at lower latitudes (6°) that's not found in the data. The evaporation of clouds at high latitudes could

offer another explanation for these missing clouds, although an episodic outflow should still be considered.

Furthermore, there are no distinguishable characteristics of an episodic outflow in the latitude vs longitude graphs provided by Figure 9. This is the case for both the simulated and observed data. Unless the episode without clouds is quite large, we will not be able to observe an obvious difference in the positions of clouds.

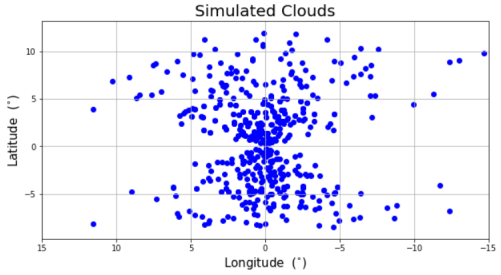

(a) Simulated Episodic Clouds

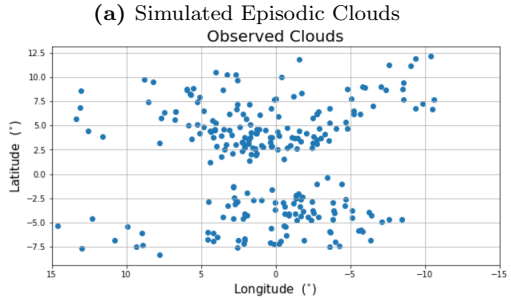

(b) Observed Clouds

Figure 9: Galactic longitude and latitude of the HI clouds for both the episodic simulation and the observed data. Notice that the simulated data lacks any obvious gaps in latitudes as seen by the velocity graphs. The same goes for the observed data.

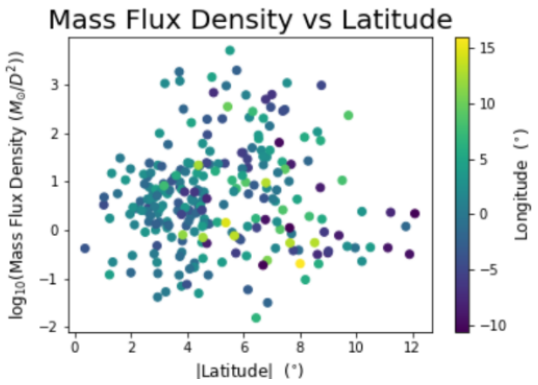

(a)

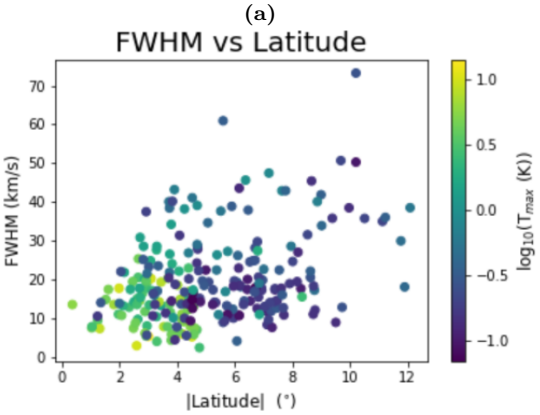

(b)

Figure 10: Figure (a) shows the $\log_{10}$ of mass flux density vs latitude, with clouds color coded by longitude. Mass flux density (M_{HI}/D^2) was plotted rather than mass in order to remove distance dependence of mass. The $\log_{10}$ was taken of this quantity to account for a few particularly high-massed clouds. Figure (b) shows FWHM vs latitude, with clouds color coded by $T_{b,peak}$.

5 Other Results

5.1 Cloud Evolution

Other outflow qualities we analyzed were the mass and FWHM of the clouds with respect to latitude. Plots of these are presented in Figure 10.

Based on Figure 10(a), there does not seem to be a relationship between mass and latitude. However, regarding Figure 10(b), there does seem to be a relationship in FWHM. The clouds' mass are not changing, yet there are observed on a larger spread of velocities as latitude increases. This led us to expect fainter clouds, a conclusion confirmed by the color-coding of Figure 10(b). This suggests that clouds are being ripped apart at high latitudes by the hot winds of the Fermi Bubbles, as supported by the "entrainment" scenario. Cold gas is hit by the hot flow, either approaching the velocity of the gas or being shredded by it, and is considered a very destructive process. Through simulations of cold gas in a hot wind, the cold gas is being torn and ionized on times scales much shorter than needed to accelerate to observed velocities (e.g., Scanna-

pieco &Brüggen 2015; Schneider Robertson 2017; Sparre et al. 2019). Given the much older acceleration model discussed in this paper, it is possible that there are other forces at play. For example, other studies show that a cloud lifetime can be prolonged through radiative cooling (Gronke & Oh 2018), thermal conduction (Brüggen & Scannapieco 2016), and magnetic fields (McCourt et al. 2015).

5.2 Clouds with Tails

A set of unusual clouds was discovered while finding the 50 clouds from this summer. These clouds had velocity gradients pointing in various directions within the Fermi Bubbles, rather than towards the galactic center, as expected. An example of such cloud is in Figure 11. Further analysis of these

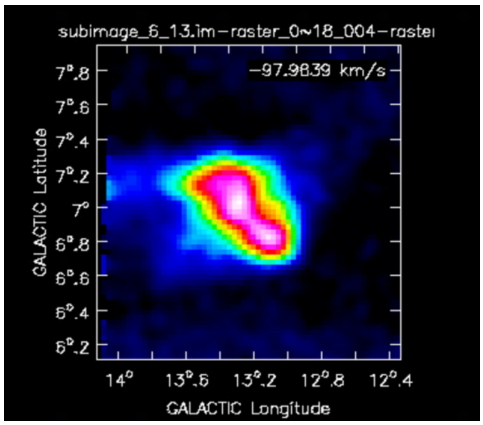

Figure 11: HI column density map of a cloud whose velocity gradient is moving away from the center of the Fermi Bubbles rather than the galactic center. Sadly, CASA has been very buggy and was not able to produce a good velocity gradient map of this cloud.

clouds and their velocity gradients could shed light on whether or not the outflow velocities are purely radial or not.

6 Conclusion

New data found both from earlier this year and during this summer have allowed us to ask key questions that may affect our understanding of the Milky Way's nuclear winds. It has been found that these neutral hydrogen clouds must have been accelerating for longer than previously calculated. Additionally, a gap in velocities at high latitudes suggest that the outflow could potentially be episodic, although this cannot be certain until more observations are made. Furthermore, clouds with velocity gradients in directions other than from the galactic center and other investigations on cloud morphology could lead to a more detailed analysis of the trajectory and development of the Milky Way's nuclear winds.

7 Acknowledgements

I would like to express my gratitude to the National Radio Astronomy Observatory and the Green Bank Observatory for hosting a research experience for undergraduates and allowing me the opportunity to be a part of this memorable research experience. I would also like to thank my mentor, Jay Lockman, for guiding me through this experience. I have learned an amazing amount this summer and I appreciate his patience and encouragement as I've worked on this project.

References

[1] Bland-Hawthorn, J., & Cohen, M. 2003, ApJ, 582, 246

[2] Bland-Hawthorn, J., Maloney, P., Sutherland, R., et al. 2019, ApJ, 886, 45

[3] Brüggen, M., & Scannapieco, E. 2016, ApJ, 822, 31

[4] Di Teodoro, E. M., McClure-Griffiths, N. M., Lockman, F. J., et al. 2018, ApJ, 855, 33

[5] Fox, A. J., Bordoloi, R., Savage, B. D., et al. 2015, ApJL, 799, L7

[6] Gronke, M., & Oh, S. P. 2018, MNRAS, 480, L111

[7] Guo F & Mathews WG 2012, ApJ, 756, 181

[8] Keeney, B. A., Danforth, C. W., Stocke, J. T., et al. 2006, ApJ, 646, 951

[9] Lockman, F. J., Di Teodoro, E. M., & McClure-Griffiths, N. M. 2020, ApJ, 888, 51

[10] McClure-Griffiths, N. M., Green, J. A., Hill, A. S., et al. 2013, ApJL, 770, L4

[11] McCourt, M., O'Leary, R. M., Madigan, A.-M.,& Quataert, E. 2015, MNRAS, 449, 2

[12] Savage, B. D., Kim, T.-S., Fox, A. J., et al. 2017, ApJS, 232, 25

[13] Scannapieco, E., & Brüggen, M. 2015, ApJ, 805, 158

[14] Schneider, E. E., & Robertson, B. E. 2017, ApJ, 834, 144

[15] Sparre, M., Pfrommer, C.,& Vogelsberger, M. 2019, MNRAS, 482, 5401

[16] Su, M., Slatyer, T. R., & Finkbeiner, D. P. 2010, ApJ, 724, 1044

[17] Veilleux, S., Cecil, G., & Bland-Hawthorn, J. 2005, ARA&A, 43, 769